Rotation-Induced Polymorphic Transitions in Bacterial Flagella

Reinhard Vogel* and Holger Stark

Institut für Theoretische Physik, Technische Universität Berlin, Hardenbergstrasse 36, 10623 Berlin, Germany

(Received 16 October 2012; published 9 April 2013)

Bacteria propel themselves with the help of rotating helical flagella. They change their swimming direction during tumbling events in order to increase, for example, their supply of nutrients (chemotaxis). During tumbling a bacterial flagellum assumes different polymorphic states. Based on a continuum model for the motor-flagellum system, we demonstrate that a changing motor torque can initiate these polymorphic transformations. In particular, we investigate the run-and-stop tumble strategy of *Rhodobacter sphaeroides* which uses a coiled-to-normal transition in its single flagellum. We also show that torque reversal in single-flagellated *Escherichia coli* generates a normal-to-curly *I* transition as observed for tumbling *E. coli* that swim with a bundle of several flagella.

DOI: 10.1103/PhysRevLett.110.158104 PACS numbers: 87.17.Jj, 87.10.Pq, 87.16.Qp, 87.85.St

The bacterial flagellum, a long helical filament, is a masterpiece of nature's ingenuity. Its hollow tube is built from thousands of copies of a single protein called flagellin which assumes two states [1–3]. This design principle is sufficient to enable a total of 12 helical or polymorphic forms. Together with a rotary motor and the connecting hook, nature provides a unique propulsion system which inspires the construction of micro- and nanorobots [4,5] moving at low Reynolds number [6]. This requires a thorough understanding of the system's biomechanics.

Bacteria such as *Escherichia coli* and *Salmonella typhimurium* propel themselves by rotating a bundle of such flagella [7]. When one of the driving motors reverses its sense of rotation, the attached flagellum leaves the bundle. It goes through a sequence of polymorphic forms while causing the bacterium to tumble. After about 0.1 s the motor switches back to the original sense of rotation and the flagellum rejoins the bundle in its normal form. The bacterium resumes its swimming path in a different direction in order to search, for example, for better food conditions, a strategy known as chemotaxis. Recent research clarified that hydrodynamic interactions are crucial for synchronizing rotating flagella and forming the flagellar bundle [8–13].

The different polymorphic forms were observed as response to external forces or torques [14–18], but also under changing solvent conditions such as *p*H value, salinity, and temperature or in mutants [19–22]. However, to date there is no theoretical model reproducing the polymorphic transitions triggered by the reversal of the driving motor torque when the bacterium tumbles. The Letter provides such a model for this unresolved and important issue based on a continuum theory which is able to treat torque-induced polymorphic transitions and using parameters adjusted to the real system.

In contrast to *E. coli* and *Salmonella*, the single flagellated bacterium *Rhodobacter sphaeroides* uses a much simpler flagellar polymorphism. It follows a run-and-stop strategy for tumbling and thereby performs chemotaxis [17,23–25]. We will investigate it first here. During swimming the flagellum assumes a right-handed normal form optimized for propelling the bacterium forward. Now, *R. sphaeroides* is able to switch off the rotary motor and the bacterium comes to a halt which can last for several seconds. The flagellum relaxes to a whiplike form referred to as open coiled. When the motor starts to rotate again, the flagellum returns into the normal form and the bacterium swims into a new random direction [17,23–25]. A first modeling of *R. sphaeroides* was presented in Refs. [26,27].

Different theoretical approaches to model flagellar polymorphism exist [2,28–33]. Here we use a generalized Kirchhoff rod theory developed in Ref. [33] to describe force-induced polymorphic transitions [15]. We combine it with a coarse-grained approach for driving the flagellum by the motor torque which is transmitted to the flagellum by the flexible hook [34]. We briefly summarize the theory. We describe the filament by the space curve $\boldsymbol{r}(s)$ parametrized by arclength s. At each point on the filament, we attach the material frame $\{\boldsymbol{e}_1, \boldsymbol{e}_2, \boldsymbol{e}_3\}$, where $\boldsymbol{t} = \boldsymbol{e}_3$ is the local tangent vector. The rotational strain vector $\boldsymbol{\Omega}$ transports the material frame along the filament, $\partial_s \boldsymbol{e}_i = \boldsymbol{\Omega} \times \boldsymbol{e}_i$. Its components determine the flagellar conformation via the local curvature $\kappa = \sqrt{\Omega_1^2 + \Omega_2^2}$, twist angle $\phi = -\arctan(\Omega_1/\Omega_2)$, and torsion $\tau = \Omega_3 + \partial_s \phi$. The Kirchhoff elastic free energy density of the deformed filament with respect to its helical ground state $\boldsymbol{\Omega}_0$ reads $\mathring{f}(\boldsymbol{\Omega}, \boldsymbol{\Omega}_0) = A/2[(\Omega_1 - \Omega_1^0)^2 + (\Omega_2 - \Omega_2^0)^2 + \Gamma(\Omega_3 - \Omega_3^0)^2]$ [35,36]. We choose the bending rigidity $A = 3.5$ pN μm^2 for *Salmonella* [15] and a twist-to-bend ratio $\Gamma = 0.7$ [33].

Following Ref. [33], we assign to each polymorphic state with helical parameters $\boldsymbol{\Omega}_n$ the Kirchhoff elastic free energy density and a ground state energy δ_n. At each rotational strain $\boldsymbol{\Omega}$, the polymorphic form with the lowest energy determines the resulting elastic free energy, $\mathring{f}_{\text{poly}}(\boldsymbol{\Omega}) = \min_n[\mathring{f}(\boldsymbol{\Omega}, \boldsymbol{\Omega}_n) + \delta_n]$. For the two helical

states of *R. sphaeroides*, we illustrate $\mathfrak{f}_{\rm poly}$ by a contour plot in Fig. 1. In addition, we introduce $\mathfrak{f}_{\rm grad} = A\xi^2(\partial_s\boldsymbol{\Omega})^2/2$, where the coherence length ξ determines the width of the transition region between two helical states, and the stretching free energy density $\mathfrak{f}_{\rm st} = K(\partial_s\boldsymbol{r})^2/2$. The length and elastic constant are adjusted, respectively, to $\xi = 0.17\ \mu$m and $K = 10^3$ pN [33]. Then the total elastic free energy of a filament with length L becomes $\mathcal{F}[\boldsymbol{r}(s),\phi(s)] = \int_0^L \mathfrak{f}_{\rm poly}(\boldsymbol{\Omega}) + \mathfrak{f}_{\rm grad}(\partial_s\boldsymbol{\Omega}) + \mathfrak{f}_{\rm st}(\partial_s\boldsymbol{r})ds$, from which one derives the elastic force and torque densities $\boldsymbol{f}_{\rm el} = -\delta\mathcal{F}/\delta\boldsymbol{r}$ and $m_{\rm el} = -\delta\mathcal{F}/\delta\phi$, respectively. For the flagellar contour $\boldsymbol{r}(s)$ and the intrinsic twist $\phi(s)$, we introduce Langevin equations, where we balance elastic and thermal forces or torques by viscous drag:

$$[\gamma_\parallel \boldsymbol{t}\otimes\boldsymbol{t} + \gamma_\perp(\mathbf{1} - \boldsymbol{t}\otimes\boldsymbol{t})]\partial_t\boldsymbol{r} = \boldsymbol{f}_{\rm el} + \boldsymbol{f}_{\rm th}, \quad (1a)$$

$$\gamma_R\partial_t\phi = m_{\rm el} + m_{\rm th}. \quad (1b)$$

Here, $\boldsymbol{t}$ is the local tangent vector. The anisotropic friction tensor is ultimately responsible for coupling rotation about the helical axis to translation and thereby creates the thrust force that pushes the bacterium forward [7]. For the friction coefficients per unit length, we choose adjusted values $\gamma_\parallel = 1.6\times10^{-3}$ pNs/μm^2, $\gamma_\perp = 2.8\times10^{-3}$ pNs/μm^2, and $\gamma_R = 1.26\times10^{-6}$ pNs [34]. As usual $\boldsymbol{f}_{\rm th}$ and $m_{\rm th}$ are Gaussian stochastic variables with zero mean that obey the fluctuation-dissipation theorem. We discretize the Langevin equations and solve them numerically [33,34].

We introduce a model bacterium for *R. sphaeroides* where we mimic the cell body by a sphere of radius $a = 1\ \mu$m at position $\boldsymbol{r}_B$. The filament is attached at the point $\boldsymbol{r}_B + a\boldsymbol{e}$ on the surface, where $\boldsymbol{e}$ is a unit vector. We drive the filament by the motor torque $\boldsymbol{M} = -M\boldsymbol{e}$, which in our coarse-grained hook model acts directly on the first material frame of the flagellum as explained in Ref. [34]. For positive M the flagellum rotates clockwise and the cell body counterclockwise, when viewed from behind. The spherical cell body moves with a velocity $\boldsymbol{v} = \boldsymbol{F}/\gamma_T$ due to the thrust force $\boldsymbol{F}$ created by the rotating flagellum and it rotates with angular velocity $\boldsymbol{\omega} = (M\boldsymbol{e} + a\boldsymbol{e}\times\boldsymbol{F})/\gamma_R$. The translational and rotational friction coefficients are, respectively, $\gamma_T = 6\pi\eta a$ and $\gamma_R = 8\pi\eta a^3$. To avoid an overlap of the filament with the cell body, we use the repulsive soft-core potential $U = F_0 a\frac{1}{12}(\frac{a}{r^{(n)}})^{12}$, where $r^{(n)} = |\boldsymbol{r}^{(n)} - \boldsymbol{r}_B|$ is the distance between a point of the filament $\boldsymbol{r}^{(n)}$ and the center of the cell body $\boldsymbol{r}_B$. The resulting interaction force enters the Langevin equations. At the cell surface, we choose its strength $F_0 = 1$ pN comparable to the typical thrust force.

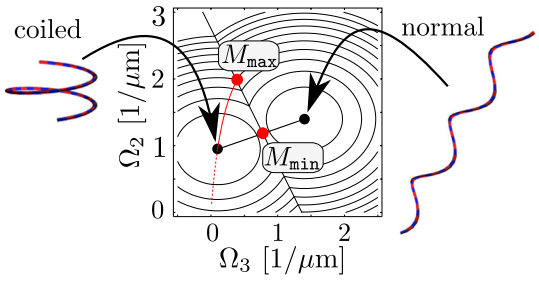

FIG. 1 (color online). Contour plot of the elastic free energy density $\mathfrak{f}_{\rm poly}$ for the two flagellar states of *Rhodobacter sphaeroides*. The red line and the characteristic torques $M_{\rm min}$ and $M_{\rm max}$ are discussed in the text.

When *R. sphaeroides* swims, the rotating flagellum is in the normal form with curvature $\kappa_n = 1.4\ \mu$m^{-1} and torsion $\tau_n = 1.4\ \mu$m^{-1} [23]. It is comparable to the normal flagellar form of *E. coli* but right-handed. The flagellum relaxes into the open coiled form when the motor torque is switched off. It has a curvature $\kappa_c = 0.95\ \mu$m^{-1} and a small pitch or torsion for which we assume $\tau_c = 0.1\ \mu$m^{-1} [17]. Alternative values in Ref. [37] do not allow a torque-induced transition as discussed in the Supplemental Material [38]. We assume the Frenet frame to be the same for both forms and choose it as the material frame so that the helical parameters for normal and coiled state become $\boldsymbol{\Omega}_{n,c} = (0, \kappa_{n,c}, \tau_{n,c})$. Since the coiled form is the ground state, we introduce a small energy density difference $\delta_n = 0.1$ pN for the normal form [33].

A torque-driven flagellum in its normal form is under compressive stress due to the generated thrust force [34]. Since the coiled form of *R. sphaeroides* has a small torsion, the thrust force is also small and the motor torque mainly twists the flagellum. It therefore expands and a coiled-to-normal transition becomes possible. To estimate the necessary torque, we argue as follows and refer details to the Supplemental Material [38]. The rotating filament experiences hydrodynamic friction such that the torque acting on the filament increases from zero at the free end towards the applied motor torque at the cell body. This results in a nonuniform deformation of the helical filament. We approximate the local deformation by calculating the uniform deformation of a helical spring with $\Omega_1 = 0$ under an applied torque and force. Since here the compressive force is small, setting it to zero directly relates curvature Ω_2 and torsion Ω_3 to each other:

$$\Gamma(\tau_0 - \Omega_3)\Omega_2 = (\kappa_0 - \Omega_2)\Omega_3. \quad (2)$$

In Fig. 1 the resulting hyperbola is indicated in the $\Omega_2 - \Omega_3$ plane as a red line in the contour plot of the elastic free energy $\mathfrak{f}_{\rm poly}$. It intersects the energy barrier between both polymorphic states at a torque value $M_{\rm max}$, meaning that we expect a fast torque-induced polymorphic transition from the coiled to the normal state for torques $M > M_{\rm max}$. The minimal energy barrier lies on the line connecting both ground states. Locally, it is reached by a torque $M_{\rm min}$, which thus is the minimal torque to initiate a polymorphic transition. Both $M_{\rm min}$ and $M_{\rm max}$ follow from the constitutive relation for the torque in the Supplemental Material [38]. Indeed, in simulations we do not observe any normal state for $M < M_{\rm min}$ while for $M > M_{\rm max}$ a

nearly complete coiled-to-normal transition occurs almost instantly. In between, the length of the normal form depends on the simulation time with a large variability indicating the importance of thermal fluctuations.

In Fig. 2 we study the dynamics of the polymorphic transition to understand the swimming and tumbling of *R. sphaeroides*. When we apply a motor torque $M = 4.5\ \mathrm{pN}\,\mu\mathrm{m} > M_{\mathrm{max}}$ at time $t = 0$, the flagellum almost instantly switches into the normal state as observed in experiments and our model bacterium starts to swim. When we reduce the motor torque to zero, the bacterium stops and the filament relaxes slowly into the coiled state. Figure 2(b) shows the applied motor torque as a function of time in blue (thick blue line). It also illustrates the temporal evolution of the flagellar conformation by color-coding the polymorphic state along the filament (arclength $s = 0, \ldots, 10\ \mu\mathrm{m}$): white for the open coiled and gray for the normal state, respectively. In Fig. 2(a) we show special snapshots of the nonuniformly deformed flagellum (thick blue line) by plotting the local values for curvature Ω_2 and torsion Ω_3 along the filament in the contour plot of the elastic free energy.

In Fig. 2(c) we show snapshots of the model bacterium during the polymorphic transition of the flagellum. At 5 ms a small part of the filament close to the cell body is already

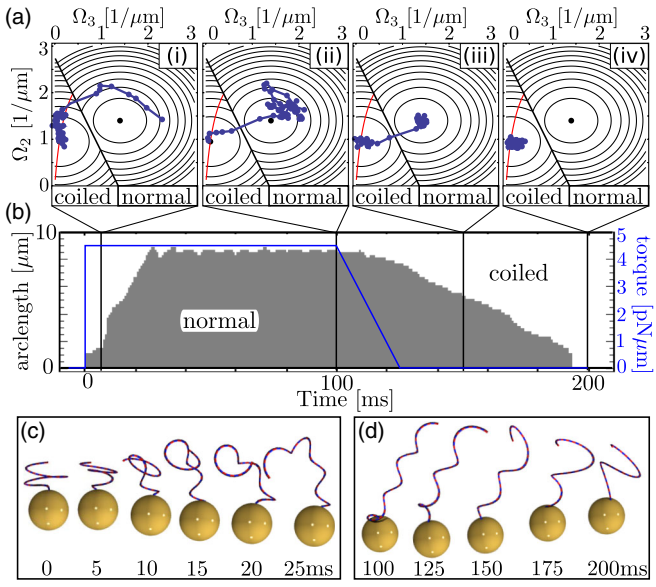

FIG. 2 (color online). Torque-driven polymorphism in *R. sphaeroides*. (a) Snapshots of the flagellar conformation (blue line with circles) plotted in $\Omega_2 - \Omega_3$ space together with the contour lines of $\mathfrak{f}_{\mathrm{poly}}$ at different times. The thin red line indicates the relation (2) valid for a force-free expansion of the helix. (b) Time protocol of the applied motor torque (thick blue line). The polymorphic state along the filament is indicated for each time from the base at arclength $s = 0$ to the tip at 10 μm in white (coiled) and gray (normal). (c) Snapshots of the filament during the coiled-to-normal and (d) the normal-to-coiled transition.

in the normal state [Fig. 2(b)]. The rest of the filament in the coiled state deforms without compressive stress as illustrated by the match of the blue filament (circles) and the red line in Fig. 2(a)(i). During the coiled-to-normal transition the height of the flagellum increases drastically from 1 to 7 μm. This means that the normal part of the flagellum expands into the remaining coiled conformation. Thus, at 25 ms, when the filament has completed its transition into the normal state (except for 10%), the flagellum is bent. A rough estimate for the transition time is given by the time $\tau_n \simeq R_n^2 L^2 \gamma_\perp / A \approx 10$ ms a disturbance needs to spread over the whole filament [33,39], where we used the radius $R_n = 0.35\ \mu$m of the normal form. From $t = 25$ to 100 ms, the filament relaxes to the straight helix. During this relaxation, the bacterium mainly reorients its swimming direction, it tumbles, as we demonstrate in the Supplemental Material [38]. We find a mean tumble angle of 35°. It decreases when the motor torque is switched on gradually. Tumbling is the least effective for a switching time of 25–50 ms, which is equal to the coiled-to-normal transition time. So the normal filament is less bent when the coiled-to-normal transition is completed. Typical tumble angles for *E. coli* are 68° [40], for *R. sphaeroides* they are reported to be smaller than for *E. coli* [23]. Finally, both Figs. 2(a)(ii) and 2(b) show that at $t = 100$ ms about 90% of the filament has transformed into the normal state. The free end stays in the coiled state since it is torque-free. However, this is not visible in the first picture of the filament in Fig. 2(d).

Starting at $t = 100$ ms, we reduce the motor torque to zero within 25 ms. Figure 2(d) shows snapshots during the normal-to-coiled transition. It starts from the free end from where the coiled form relaxes towards the cell body as observed in experiments [25]. However, compared to the coiled-to-normal transition, now the filament takes a different path as Fig. 2(a)(iii) illustrates. It crosses the energy barrier between both states where it is smallest and relaxes slowly into the coiled state during about 100 ms. The relaxation time decreases with barrier height and, hence, with increasing ground state energy δ_n but also with increasing coherence length ξ in $\mathfrak{f}_{\mathrm{grad}}$. A lower bound is the spreading time $\tau_c \simeq R_c^2 L^2 \gamma_\perp / A = 80$ ms of the coiled filament. Finally, we note that during this process the cell body is pulled backwards since the height of the helical state reduces drastically.

Flagella in tumbling *E. coli* or *Salmonella* go through several polymorphic forms [40]. We now investigate if our theory can describe such a process for the single-flagellated model bacterium. *E. coli* with just one flagellum have indeed been observed in experiments [40]. Each flagellum is made of 11 protofilaments, which exist in either the *R* or *L* state [1–3]. So 12 different helical forms of the flagellum are possible, which one labels by the number n_R of *R*-state protofilaments. During tumbling of *E. coli* or *Salmonella* the filament transforms from the

normal ($n_R = 2$) to the semicoiled ($n_R = 4$) and finally to the curly I ($n_R = 5$) form. We complement them by the coiled form ($n_R = 3$) which is situated between the normal and the semicoiled state. We take their respective curvatures κ_{n_R} and torsions τ_{n_R} from Calladine's formulas as given in Ref. [33]. Since the material frame is attached to the molecular structure, the Frenet frame (defined by curvature and torsion) successively rotates by an angle of $\delta\phi = 2\pi/22$ against the material frame when n_R is increased by one. We explain details of this effect in the Supplemental Material [38]. For two polymorphic states we can neglect it; however, for four states it becomes important. Therefore, we use the rotational strain vector $\mathbf{\Omega}_{n_R} = \{\kappa_{n_R} \sin[(2 - n_R)\frac{\pi}{11}], \kappa_{n_R} \cos[(2 - n_R)\frac{\pi}{11}], \tau_{n_R}\}$ for the four helical ground states in agreement with experimental observations [41]. The sign of the twist angle is chosen such that in the tumbling phase the motor torque unwinds the normal form. As ground state energies we assume $\delta_{n_R} = (n_R - 2)0.1$ pN [33].

We add here an additional hook-bending torque of the form $M_{\text{hook}}(\alpha) = 0$ for $\alpha \leq \alpha_0$ and $M_{\text{hook}}(\alpha) = M_H(\frac{1}{\cos(\alpha)} - \frac{1}{\cos(\alpha_0)})$ for $\alpha > \alpha_0$, that applies to the first material frame of the filament, where α is the angle between the motor-torque direction $\boldsymbol{e}$ and the first tangent of the filament. For $\alpha > \alpha_0$, it prevents the surface-attached end of the filament to point into the cell body. In the simulations we choose $\alpha_0 = \pi/4$ and $M_H = 3.5$ pN μm.

Figure 3(a) shows the time protocol of the applied motor torque (red line) and the polymorphic form along the filament during our simulation. We rotate the filament in the normal state by a torque $M = -3.4$ pN μm, which is in good agreement with the motor torque of 3.6 pN μm reported for *E. coli* in Ref. [7]. Then, within 15 ms we linearly increase M up to a value of $+3.4$ μm. When the torque reaches its maximum value, we observe a rapid transition of the filament into the curly I form of the bacterial flagellum. The snapshots of the filament in Fig. 3(b) at $t = 21$ and 22 ms clearly show the region at the bottom where the helicity between the normal and curly I state changes its sign. The region then propagates to the tip of the filament. After 40 ms we reverse the motor torque again and the filament transforms back to the normal state. The two intermediate states, coiled and semicoiled, are only visible at the boundary between the normal and curly I form. On first sight our snapshots of the normal-to-curly I transition look similar to experimental pictures in Ref. [40]. However, the small kink angle between the normal and curly I form visible at 26 ms in Fig. 3(b) is much more pronounced in experiments as a "dogleg bend" [14]. The flagellar polymorphism in *E. coli* is governed by a complex energy landscape determined, for example, by the ground state energies δ_{n_R}. In future work we hope to reproduce these dogleg bends by tuning the relevant parameters appropriately.

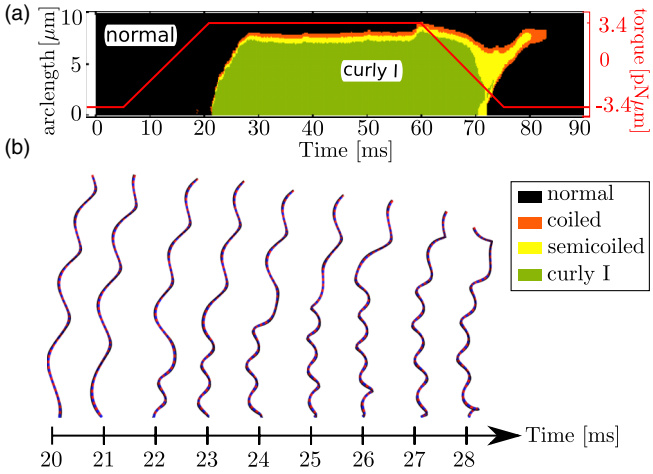

FIG. 3 (color online). Torque-driven polymorphism in a single-flagellated *E. coli*. (a) Time protocol of the applied motor torque (red line) and color-coded polymorphic state along the filament. (b) Snapshots of the filament during the normal-to-curly I transition.

In conclusion, bacterial polymorphism is essential in the tumbling events of bacteria. Here we presented a continuum model of the bacterial flagellum, which is able to describe polymorphic transformations in response to an applied motor torque. Our approach successfully applies to the run-and-stop strategy of *R. sphaeroides*. It predicts a minimum motor torque needed for a fast coiled-to-normal transition and localizes the tumbling event when the bent flagellum relaxes to the straight helix. Details of our findings should be observable in an experiment.

Furthermore, we demonstrated a normal-to-curly I transition for a single-flagellated *E. coli* that is observed during tumbling of multiflagellated *E. coli*. Our approach is crucial for modeling and understanding the complete tumbling event of *E. coli* including flagellar bundling. It gives a striking example that biomechanical modeling helps to elucidate the sophisticated design principles of nature.

We acknowledge discussions with G. Gompper and R. Winkler. We thank the VW foundation for financial support within the program "Computational Soft Matter and Biophysics" (Grant No. I/83 942) and the Research Training Group GRK 1558 funded by the Deutsche Forschungsgemeinschaft.

*reinhard.vogel@tu-berlin.de

[1] S. Asakura, Adv. Biophys. **1**, 99 (1970).
[2] C. R. Calladine, Nature (London) **255**, 121 (1975).
[3] C. R. Calladine, J. Mol. Biol. **118**, 457 (1978).
[4] B. J. Nelson, I. K. Kaliakatsos, and J. J. Abbott, Annu. Rev. Biomed. Eng. **12**, 55 (2010).
[5] K. E. Peyer, A. W. Mahoney, L. Zhang, J. J. Abbott, and B. J. Nelson, in *Microbiorobotics: Biologically Inspired Microscale Robotic Systems*, edited by M. J. Kim,

A. A. Julius, and E. Steager (Elsevier, New York, 2012), pp. 165–199.
[6] E. Lauga and T. R. Powers, Rep. Prog. Phys. **72**, 096601 (2009).
[7] H. C. Berg, *E. coli in Motion* (Springer, New York, 2004).
[8] M. J. Kim and T. R. Powers, Phys. Rev. E **69**, 061910 (2004).
[9] M. Reichert and H. Stark, Eur. Phys. J. E **17**, 493 (2005).
[10] P. J. A. Janssen and M. D. Graham, Phys. Rev. E **84**, 011910 (2011).
[11] S. Y. Reigh, R. G. Winkler, and G. Gompper, Soft Matter **8**, 4363 (2012).
[12] N. Watari and R. G. Larson, Biophys. J. **98**, 12 (2010).
[13] S. E. Spagnolie and E. Lauga, Phys. Rev. Lett. **106**, 058103 (2011).
[14] R. M. Macnab and M. K. Ornston, J. Mol. Biol. **112**, 1 (1977).
[15] N. C. Darnton and H. C. Berg, Biophys. J. **92**, 2230 (2007).
[16] N. C. Darnton, L. Turner, S. Rojevsky, and H. C. Berg, J. Bacteriol. **189**, 1756 (2006).
[17] D. S. Shah, T. Perehinec, S. M. Stevens, S. I. Aizawa, and R. E. Sockett, J. Bacteriol. **182**, 5218 (2000).
[18] C. R. Calladine, B. F. Luisi, and J. V. Pratap, J. Mol. Biol. **425**, 914 (2013).
[19] R. Kamiya and S. Asakura, J. Mol. Biol. **106**, 167 (1976).
[20] E. Hasegawa, R. Kamiya, and S. Asakura, J. Mol. Biol. **160**, 609 (1982).
[21] H. Hotani, J. Mol. Biol. **156**, 791 (1982).
[22] S. Kanto, H. Okino, S. Aizawa, and S. Yamaguchi, J. Mol. Biol. **219**, 471 (1991).
[23] J. P. Armitage and R. M. Macnab, J. Bacteriol. **169**, 514 (1987).
[24] J. P. Armitage and R. Schmitt, Microbiology **143**, 3671 (1997).
[25] J. P. Armitage, T. P. Pitta, M. A.-S. Vigeant, H. L. Packer, and R. M. Ford, J. Bacteriol. **181**, 4825 (1999).
[26] E. Lobaton and A. Bayen, in *Proceedings of the American Control Conference, 2007 (ACC '07)* (IEEE, New York, 2007), pp. 455–461.
[27] E. J. Lobaton and A. M. Bayen, IEEE Trans. Control Syst. Technol. **17**, 907 (2009).
[28] R. E. Goldstein, A. Goriely, G. Huber, and C. W. Wolgemuth, Phys. Rev. Lett. **84**, 1631 (2000).
[29] D. Coombs, G. Huber, J. O. Kessler, and R. E. Goldstein, Phys. Rev. Lett. **89**, 118102 (2002).
[30] S. V. Srigiriraju and T. R. Powers, Phys. Rev. Lett. **94**, 248101 (2005).
[31] H. Wada and R. R. Netz, Europhys. Lett. **82**, 28 001 (2008).
[32] C. Speier, R. Vogel, and H. Stark, Phys. Biol. **8**, 046009 (2011).
[33] R. Vogel and H. Stark, Eur. Phys. J. E **33**, 259 (2010).
[34] R. Vogel and H. Stark, Eur. Phys. J. E **35**, 1 (2012).
[35] A. E. H. Love, *A Treatise on the Mathematical Theory of Elasticity* (Dover, New York, 1944), Vol. 4.
[36] L. D. Landau and E. M. Lifshitz, *Theory of Elasticity* (Pergamon, New York, 1986).
[37] M. Fujii, S. Shibata, and S. I. Aizawa, J. Mol. Biol. **379**, 273 (2008).
[38] See Supplemental Material at http://link.aps.org/supplemental/10.1103/PhysRevLett.110.158104 for movies of the simulations of *R. sphaeroides* and the single flagellated *E. coli*, and for further informations on the elastic free energy density for *R. sphaeroides*, the elastic distortion of a torque-driven helical filament, the tumbling of *R. sphaeroides*, and the rotational strain vector for different polymorphic states.
[39] C. W. Wolgemuth, T. R. Powers, and R. E. Goldstein, Phys. Rev. Lett. **84**, 1623 (2000).
[40] L. Turner, W. S. Ryu, and H. C. Berg, J. Bacteriol. **182**, 2793 (2000).
[41] H. Hotani, J. Mol. Biol. **106**, 151 (1976).